Measurement of the Nuclear Dependence of the EMC Effect at large x.

R. Ent, H. Fenker, D. Gaskell (Spokesperson), M. Jones, A. F. Lung, D. J. Mack, D. G. Meekins, J. Roche, G. Smith
Jefferson Laboratory, Newport News, VA

J. Arrington (Spokesperson), D. F. Geesaman, K. Hafidi, R. J. Holt, H. E. Jackson, D. H. Potterveld, P. E. Reimer, E. Schulte, B. Zeidman, X. Zheng
Argonne National Laboratory, Argonne, IL

M. E. Christy, C. E. Keppel
Hampton University, Hampton, VA

G. Niculescu, I. Niculescu
James Madison University, Harrisonburg, VA

R. Asaturyan, H. Mkrtchyan, T. Navasardyan, V. Tadevosyan
Yerevan Physics Institute, Armenia

(Dated: December 2, 2003)

Abstract

We propose to measure inclusive electron scattering from ^{2}H and several nuclei spanning the mass range from ^{7}Li to ^{197}Au at high x ($0.5 < x < 0.9$) and at large Q^2 ($\approx 4 - 7$ GeV^2). In the large x region, the rising EMC ratio as x approaches 1.0 is typically attributed to binding and Fermi motion effects. Mean–field calculations in this region, while often failing quantitatively, describe the qualitative behavior rather well. These calculations predict little A-dependence to the cross–over where the EMC ratio rises above unity at $x \approx 0.8$. There is a dearth of data in the high x region due to the typical requirements that measurements be made at $W > 2$ GeV, and hence extremely large Q^2, to ensure that one is in the deep inelastic regime. However, recent results show that the high x cross–over has significant A-dependence, even for rather heavy nuclei. This experiment will take advantage of the recently observed scaling of the EMC ratios in the resonance region to make precision measurements of the EMC ratios for a variety of nuclei at high x. We will place particular emphasis on the A-dependence of the high x cross–over.

I. INTRODUCTION AND MOTIVATION

A. The EMC Effect

Since the original observation of the modification of structure functions in nuclei by the European Muon Collaboration [1], there has been intense theoretical and experimental activity aimed at understanding nuclear effects in parton distribution functions. Twenty years later, these nuclear effects are still not fully understood. Several reviews of the EMC effect have appeared in the literature (for example, see [2] and [3]), so we will not focus on a detailed description here, but review some of the main features, in particular as they pertain to this proposal.

Figure 1 shows the ratio of the inclusive lepton Deep Inelastic cross section from iron to that from deuterium as measured by the EMC collaboration [1], the BCDMS collaboration [4], and SLAC experiments E87 [5] and E139 [6]. The x-dependence of the cross section ratio is typically broken down into three regions: the region $x < 0.1$, where the nuclear cross section is suppressed (the shadowing region), the small enhancement at $0.1 < x < 0.3$, and the large suppression at $x > 0.3$. There is, in addition, a fourth region at $x > 0.7$ where the EMC ratio increases and becomes larger than 1.0 at $x \approx 0.8$. This latter region is often ignored for two reasons. First, there is a lack of high precision data in this region due to the kinematic constraints employed ($W^2 > 4$ GeV^2, requires extremely large Q^2 values at large x) to ensure that one is in the Deep Inelastic Scattering (DIS) regime. At high x, these constraints are difficult to fulfill, requiring very high energies and long experiments. The second reason for the lack of interest in the high x region is that it is assumed to be easily described in terms of nuclear Fermi motion and binding effects, requiring little exotic or new physics. However, it is important to note that these "conventional nuclear physics" effects are, in fact, important throughout the full x range of the EMC effect. Precision data at high x can serve as a strict constraint on models that attempt to include standard nuclear effects in other x regions.

It is also worth noting that there is a significant A-dependence in the *size* of the EMC effect in the first three regions described above ($x < 0.7$). However, the *shape* of the structure function ratio as a function of x in those regions changes very little: the points where the ratio crosses unity at $x \approx 0.1$ and $x \approx 0.3$ and the position of the minimum at $x \approx 0.7$ are virtually the same for all nuclei. This has lead to a situation where calculations of the EMC effect often treat nuclei as nuclear matter which is then scaled to lower density. We will show later that this approach, which seems well motivated at $x < 0.7$ may be inadequate when one examines the high x region in more detail.

The large x region can be intuitively understood in terms of a simple x rescaling due to Fermi motion of the bound nucleon. For a stationary nucleon, Bjorken $x = Q^2/(2p \cdot q)$ reduces to $Q^2/(2m_N\nu)$. However, a nucleon bound in the nucleus has an effective x given by,

$$x' = \frac{Q^2}{2p' \cdot q} \,, \tag{1}$$

where p' is the 4–momentum of the bound nucleon and $p'^2 \neq m_N^2$. In this case, for a given $x = Q^2/(2m_N\nu)$, x' is shifted lower by an amount $\langle\epsilon\rangle/m_N$, where $\langle\epsilon\rangle$ is the mean value of the nucleon separation energy [3]. The shift of x' to smaller values, where the structure function is larger, implies that the structure function ratio should increase. In this model, the A-dependence at large x is largely determined by the separation energy, ϵ, which can be

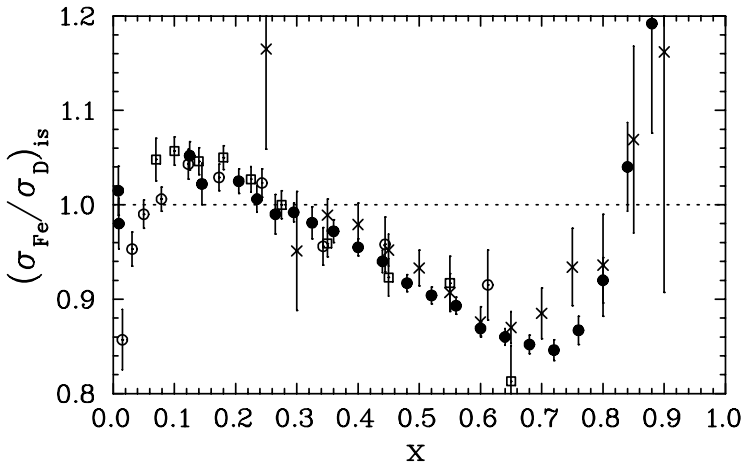

FIG. 1: $(\sigma_A/\sigma_{^2H})$ ratios as a function of x from EMC (hollow circles), SLAC (crosses and solid circles), and BCDMS (squares). The data have been averaged over Q^2 and corrected for neutron excess. The SLAC and BCDMS points show $(\sigma_{Fe}/\sigma_{^2H})$ while the EMC points show $(\sigma_{Cu}/\sigma_{^2H})$

related to the average momentum of the bound nucleon via the Koltun sum rule,

$$\langle\epsilon\rangle + \frac{\langle\vec{p}^2\rangle}{2m_N} = 2\mu \ , \tag{2}$$

where μ is the chemical potential of -8 MeV/nucleon [7]. Since the Fermi momentum of the bound nucleon is taken to scale as the nuclear density, it (and hence the high x behavior of the structure function ratio) should change very little for heavy ($A \geq 12$) nuclei. Initial calculations of the nuclear dependence of electron scattering cross sections (before the experimental observation of the EMC effect) were done in a similar (although not identical) context [8, 9], and while they predict the wrong behavior at low x, correctly predict the steep rise in the structure function ratios at $x > 0.7$.

The above simple picture is useful to gain an intuitive understanding of the high x behavior of the EMC ratio, but it should be noted that more sophisticated calculations also predict similar features. For example, Marco *et al.* [10] calculate the EMC effect in terms of an interacting Fermi sea and include the effects of extra ρ and π meson contributions to the structure functions. Their approach starts from relativistic nucleon spectral functions in an attempt to avoid the somewhat *ad hoc* corrections that often are necessary in non–relativistic mean field calculations. The results of their calculations for ^{6}Li, ^{12}C, ^{40}Ca, and ^{56}Fe are shown in Fig. 2 where the ratio of F_2/A to F_2 for the isospin averaged free nucleon (ignoring Fermi motion in deuterium) is plotted. Clearly, the expectations from the simple Fermi–motion arguments above appear to be born out. The EMC ratio rises rapidly for $x > 0.7$, and the high x cross–over changes very little as A increases from 6 to 56. Any change in the high x cross–over one can discern is a trend for the cross–over to move to smaller x for large A. The agreement with the data is rather poor at large x, but this can be attributed to the fact that calculations in this regime are quite sensitive to the structure function of deuterium in the denominator, and the results shown ignore the Fermi motion of the nucleons in the deuteron. Nonetheless, including deuteron Fermi–motion effects will improve the quantitative agreement with the data, but will not change the trend, since at each x, the correction will be common to all heavier nuclei. It is worth noting that this calculation also underscores the fact that these standard nuclear physics effects are

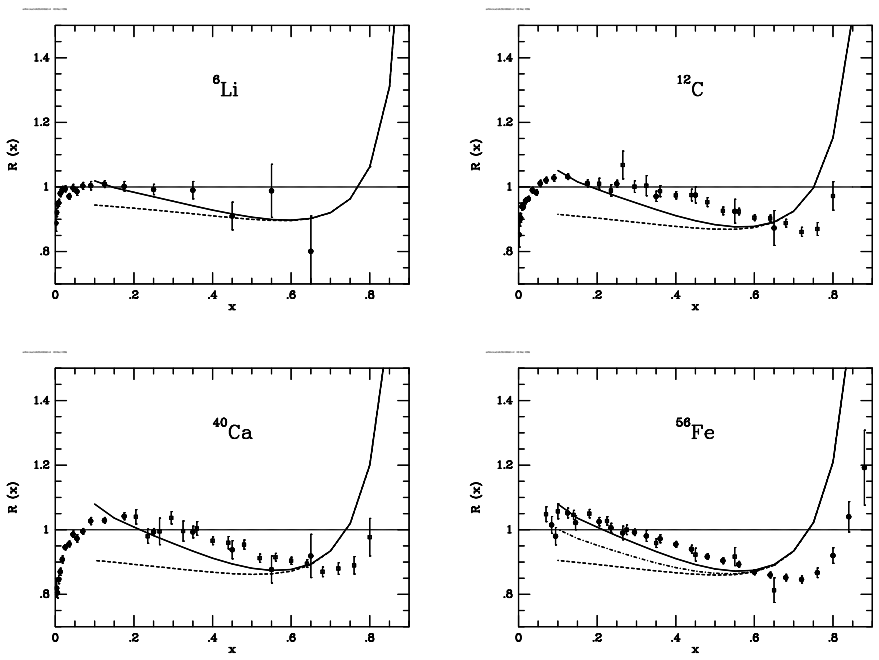

FIG. 2: Calculation of the EMC effect from Marco *et al.* [10]. The calculation was done in terms of a relativistic, mean–field model. The solid line is the full calculation which includes contributions from pions and rhos in the nucleus, while the dashed line is the contribution from the nucleons only (the dot–dashed line in ^{56}Fe includes contributions from nucleons and pions). The calculations are compared to data from SLAC experiment E139 (circles), BCDMS (squares for ^{56}Fe) and NMC (squares ^{6}Li, ^{12}Ca, and ^{40}Ca). Note that $R(x)$ is the ratio of nuclear to *nucleon* structure functions, i.e., ignoring Fermi motion effects in deuterium.

important not just at very large x, but throughout the EMC effect region. There is a clear modification of the structure function ratio down to $x = 0.1$.

Another fully relativistic calculation of the EMC effect by Gross and Liuti [11], however, predicts a rather different behavior at large x. In this case, the cross–over is predicted to shift to higher x for large A. The position of the high x crossover for the calculations of Marco *et al.* and Gross and Liuti are shown in Fig. 3. The absolute position of the high x cross–over is somewhat different, but the important feature of this plot is that, for $A \geq 12$, the two calculations do not even agree on the trend in terms of the x position of the cross–over with increasing A. Both Gross and Liuti and Marco *et al.* use fully relativistic nucleon spectral functions, and furthermore include binding effects through an explicit dependence of the nucleon structure function on the nucleon momentum. While the calculations of Marco *et al.* include additional contributions from pions and rhos, this has little or no apparent effect in the high x ($x > 0.6$) region. The fact that these two calculations which seem to start with similar approaches can result in strikingly different qualitative behavior at high x is a clear indication of the utility of high precision data in this region to test and constrain models of the nuclear dependence of Deep Inelastic Scattering. This becomes especially important in light of recent results that observe an A-dependence to the high x behavior of the EMC effect.

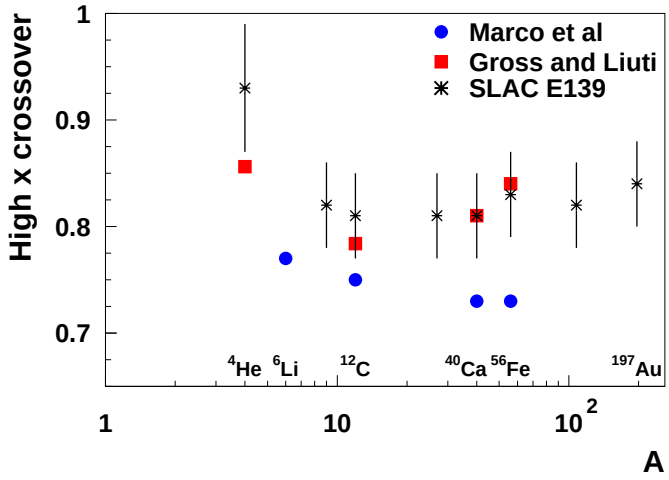

FIG. 3: Position of the high x cross–over as a function A from the calculations of Marco *et al.* [10] and Gross and Liuti [11]. The cross–over estimated from SLAC E139 data [6] is also shown for comparison. Despite the fact that the calculations include Fermi motion and binding as the dominant contributions at large x, they predict different trends for the position of the cross–over as A increases.

B. Existing Data at Large x

The most complete measurements of the EMC effect come from SLAC experiment E139 [6]. They measured ratios to deuterium for ^{4}He, ^{9}Be, ^{12}C, ^{27}Al, ^{40}Ca, ^{56}Fe, ^{108}Ag, and ^{197}Au targets for three Q^2 bins (Q^2=2 and 5 GeV^2 for $x < 0.3$; Q^2=2, 5, and 10 for $0.3 \leq x \leq 0.5$; Q^2=5 and 10 for $x > 0.5$). In addition to measuring the x-dependence, E139 examined the Q^2-dependence and A-dependence of the effect. They found no significant Q^2-dependence in the measured cross section ratios. The ratio does have a strong target dependence which, at fixed x, can be well described as a function of mass number ($\sigma_A/\sigma_{2H} = C(x)A^{\alpha(x)}$, where their fit yields $C(x) \approx 1$) or as a function of the average nuclear density, ρ ($\sigma_A/\sigma_{2H} = D(x)[1 + \beta(x)\rho(A)]$, with $\beta(x) \approx 1$). For the SLAC analysis ρ is taken to be the nuclear density (nucleons/fm^3) determined assuming a uniform sphere with a radius equal to the RMS electron scattering charge radius [6, 12]. As seen in Fig. 4, despite the significant A-dependence at fixed x, there is little apparent change in the *shape* of the cross section ratios as a function of x. More specifically, it can be seen that the second cross–over point at low x (near 0.3) is constant, though poorly determined, while the position of the minimum at $x \approx 0.7$ changes very little.

A more recent extraction of the EMC ratio is shown in Fig. 5 [13]. In this figure, the cross section ratio has been extracted using data taken in the resonance region during JLab experiment E89-008. Also shown are SLAC E139 data for comparison. Note that in this figure, the ratios are plotted as a function of the Nachtmann variable $\xi = 2x/(1+\sqrt{1+4M^2x^2/Q^2})$. At large Q^2, $\xi \to x$, so in the Bjorken limit shares the interpretation of the momentum fraction carried by the struck quark. However, at finite Q^2, using ξ reduces the effects of scaling violations associated with target mass corrections [14].

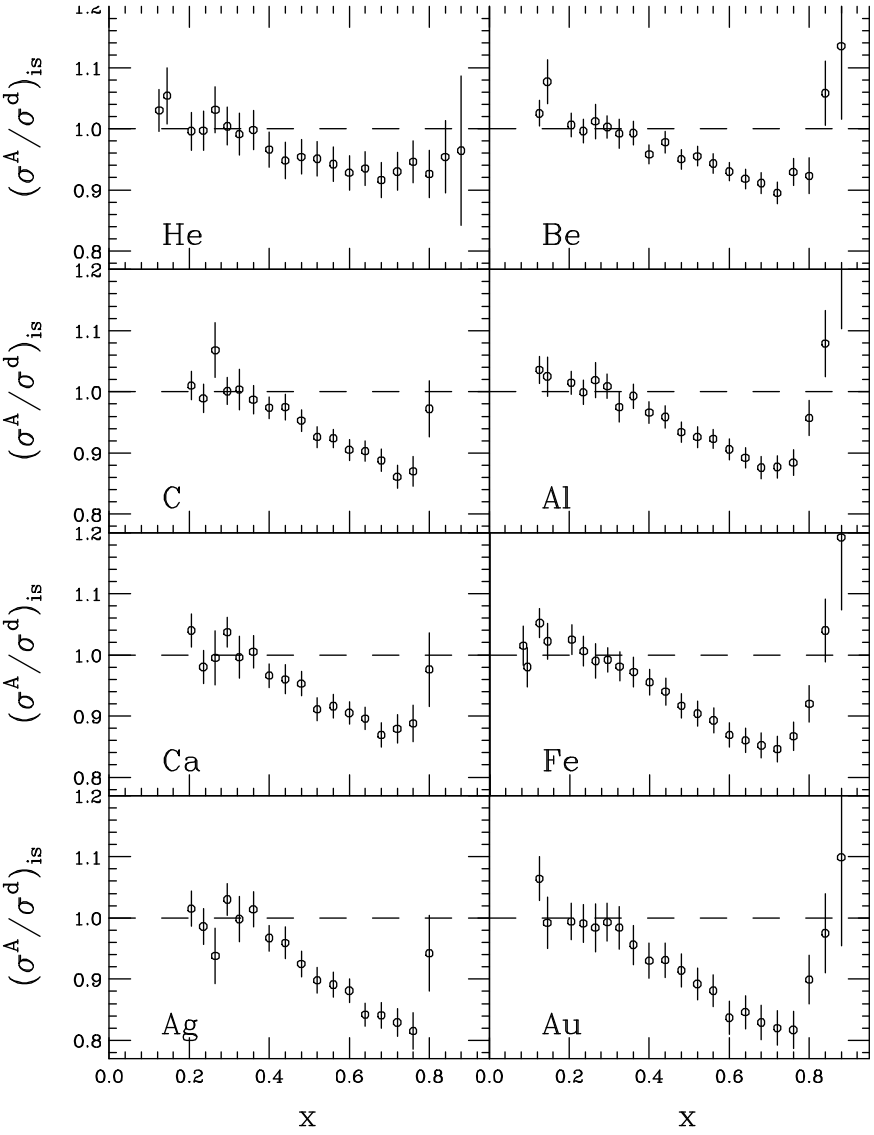

FIG. 4: (σ_A/σ_{2H}) ratios as a function of x from SLAC E139 for several nuclei. The data have been averaged over Q^2 and corrected for neutron excess.

The first important feature of Fig. 5 is that, where the resonance data overlaps the SLAC DIS data, the agreement is excellent for all nuclei shown. This result in and of itself is interesting in that it demonstrates that nuclear effects in the resonance region are identical to those in the Deep Inelastic regime. The second and perhaps more important point is that the improved coverage at large ξ allows one to see that that the shape of the EMC ratio for $\xi > 0.7$ is A-dependent, even for rather heavy nuclei. Looking at the cross–over at large ξ, one can see that for ^{56}Fe and ^{197}Au it shifts to larger ξ when compared to ^{12}C. This behavior is in stark contrast to the naive expectation as outlined in Eq. 1. In that simple picture, x' is shifted by an amount $\langle\epsilon\rangle/m_N$. Since we expect the magnitude of the mean separation energy to, if anything, increase for larger A, we might naively expect the cross–over to shift to lower x. It is perhaps not surprising that this simple picture fails quantitatively, but as we have seen, this is also a feature of other more sophisticated, mean–field calculations. This

indicates that the EMC ratio at large ξ is quite sensitive to the details of nuclear structure and binding models and precision measurements of such a quantity would undoubtedly constrain and test state–of–the–art models of nuclei.

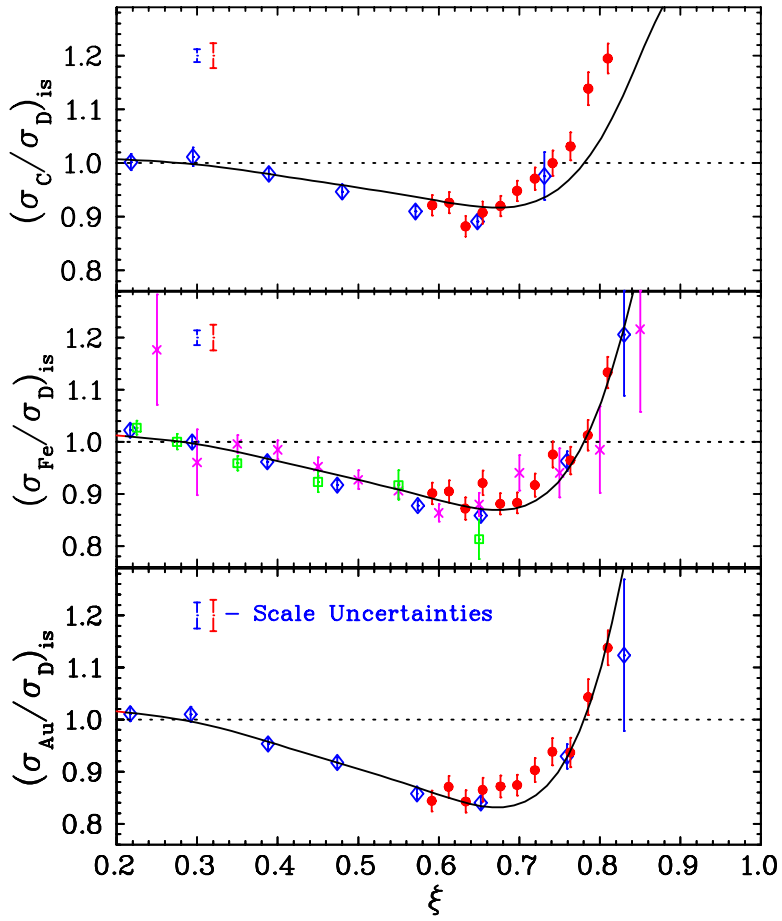

FIG. 5: $(\sigma_A/\sigma_{^2H})$ ratios as a function of ξ ($= x$ at large Q^2) from JLab Experiment E89-009 for carbon, iron, and gold (closed circles). Also shown are data from SLAC E139 (open diamonds) and BCDMS (open squares), plotted as a function of ξ instead of x, and with coulomb corrections applied. The E89-009 EMC ratio has been formed using resonance region data ($1.2 < W^2 < 3.0$, $Q^2 \approx 4.0$ GeV^2). The solid line is a fit that assumes a constant shape in ξ, but allows for A-dependence in the *size* of the cross section ratio. Clearly, such a fit is inadequate for the ^{12}C data at high ξ.

II. KINEMATIC COVERAGE, SCALING, AND DUALITY

This experiment will measure the EMC effect for nuclei from ^{7}Li to ^{197}Au, for $x > 0.5$ and $Q^2 > 4$ GeV^2. In addition, the structure functions and EMC ratios for a subset of the targets will be taken as a function of Q^2 to measure any deviations of the structure function from pQCD evolution at low Q^2 values. Figure 6 shows the proposed kinematic coverage at 6 GeV ($\theta \leq 45°$) as a function of x and Q^2. The dark (blue) points denote the x–Q^2 region for which we will take data for all nuclear targets and for which we will measure the EMC effect.

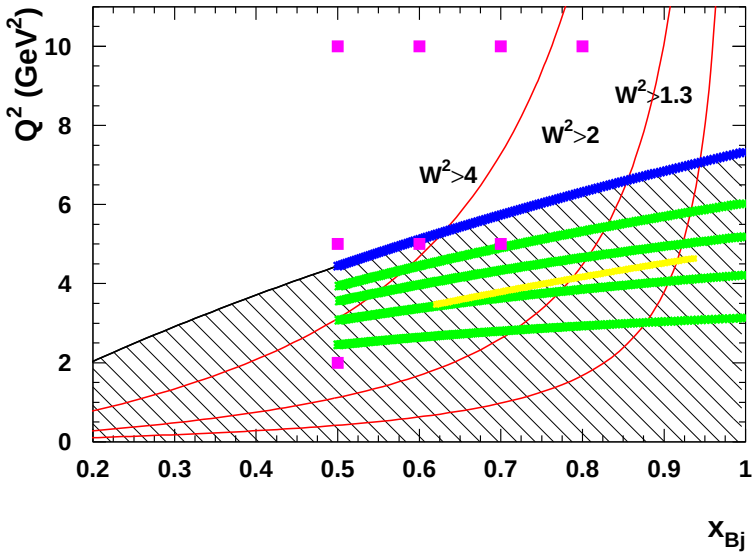

FIG. 6: Overview of the proposed kinematics. The dark (blue) lines indicate the kinematic coverage for all targets. The solid red lines correspond to W^2=1.3, 2.0, and 4.0 GeV^2 for a 6 GeV beam. Also shown are the kinematics for the JLab EMC effect measurement shown in Fig. 5 (small, yellow symbols). The SLAC E139 kinematics for $x \geq 0.5$ are also shown (solid, magenta squares). The green lines indicate kinematics for which we will take data with a subset of targets to examine the Q^2-dependence of the structure functions and target ratios.

The dark (red) lines mark the $W^2 = 4$ GeV^2, $W^2 = 2$ GeV^2, and $W^2 = 1.3$ GeV^2 limits. Clearly, a significant portion of the data will be at $W^2 < 4$ GeV^2, below what is typically considered the DIS regime. However, this constraint need no longer be so stringently applied with the observation, shown in Fig. 5, that the nuclear dependence of the cross sections as measured in the DIS region is identical to that measured in the resonance region.

The agreement between DIS and resonance region measurements of the EMC effect is perhaps not so surprising in light of measurements of scaling of the structure functions in the resonance region. Figure 7 shows the resonance region structure functions for hydrogen [15], deuterium [16], and iron [17]. Each data symbol corresponds to a different range of Q^2 (higher Q^2 ranges at higher ξ). Also shown are parameterizations of the structure functions from MRST [18] and NMC [19]. In the proton case, one can see scaling of the structure functions if one averages over the resonance structure. In the deuterium case, one can see better local agreement with scaling since most of the resonance structure, aside from the Δ, is washed out by the Fermi motion of the bound nucleons. The iron data shows even better agreement with scaling with all signs of the Δ resonance almost completely eliminated.

The previous data on duality in the proton (and nuclear) structure functions indicate that any deviations from perturbative behavior of the structure function should be small over most of the kinematics of this measurement. Extensive studies of duality in the proton (unpolarized) structure functions show that deviations from pQCD behavior are $< 10\%$ down to $Q^2 \approx 0.5$ GeV^2 when averaged over individual resonances [15, 21]. There are indications

that duality holds even better for nuclei, as the structure function moments deviate from perturbative behavior at $Q^2 \approx 2$ GeV^2 for the proton [22], but $Q^2 < 1$ GeV^2 for nuclei [23]. In addition, for nuclei the structure function need not be averaged over a resonance region to reproduce the perturbative behavior (Fig. 7 and Refs. [13, 17, 24]).

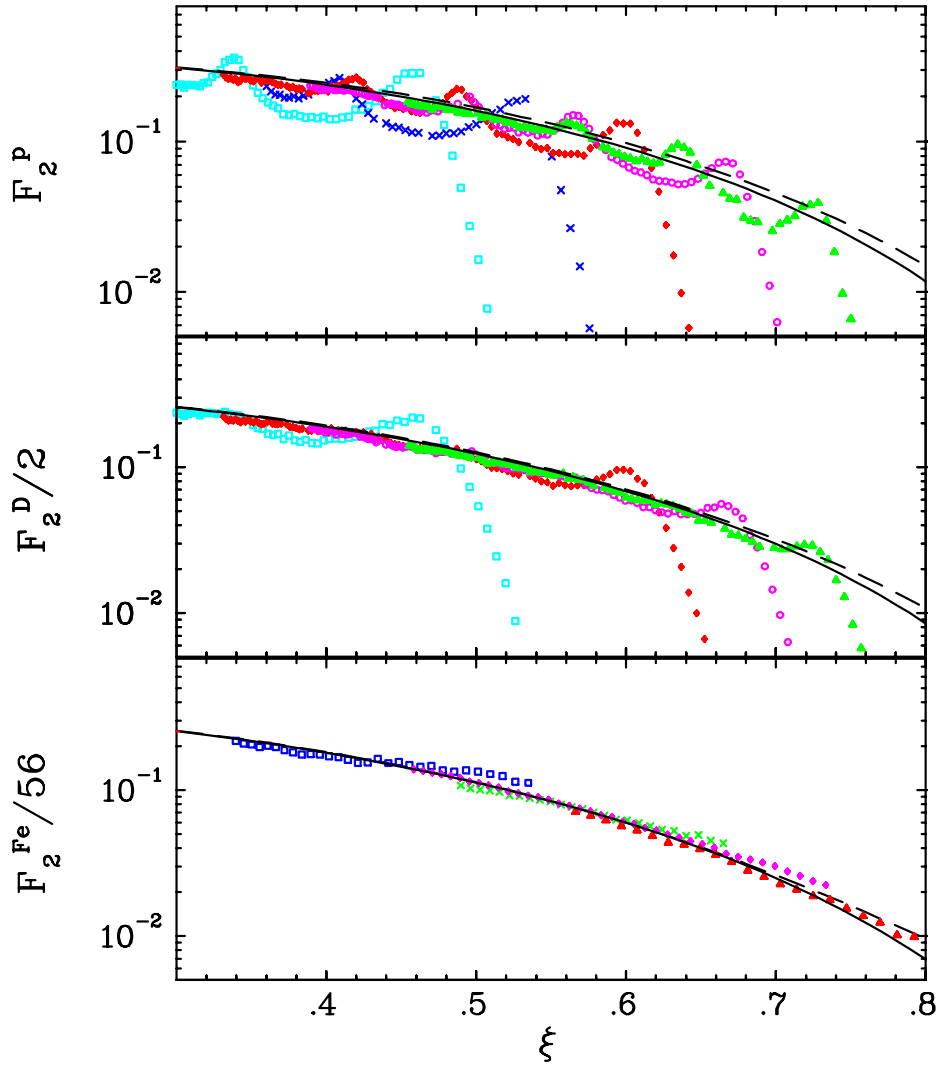

FIG. 7: Resonance region structure functions for hydrogen, deuterium, and iron. For hydrogen, the elastic peak is excluded, for deuterium the quasielastic peak is subtracted from the data, and for iron there is a cut ($W^2 > 1.3$) to exclude the quasielastic contributions.

Figure 8 shows the Q^2-dependence of the structure function for deuterium at fixed values of ξ from JLab experiment E89-008 [17] and SLAC measurements [20]. The data at $W^2 > 4$ GeV^2 are in the DIS region and show no deviations from logarithmic scaling. The data in the resonance region at $Q^2 > 3$ GeV^2 deviate from logarithmic QCD scaling by $< 10\%$ for all ξ measured. These deviations decrease with increasing Q^2 and the structure functions eventually become consistent with logarithmic pQCD scaling, even though W^2 is smaller than the value typically associated with the DIS regime. The success of ξ-scaling in deuterium at extremely low values of W (above the QE peak) and relatively low momentum transfers leads us to believe that the very precise scaling observed in the DIS region should

extend below $W^2 = 4$ GeV^2, especially for the larger Q^2 values of this measurement.

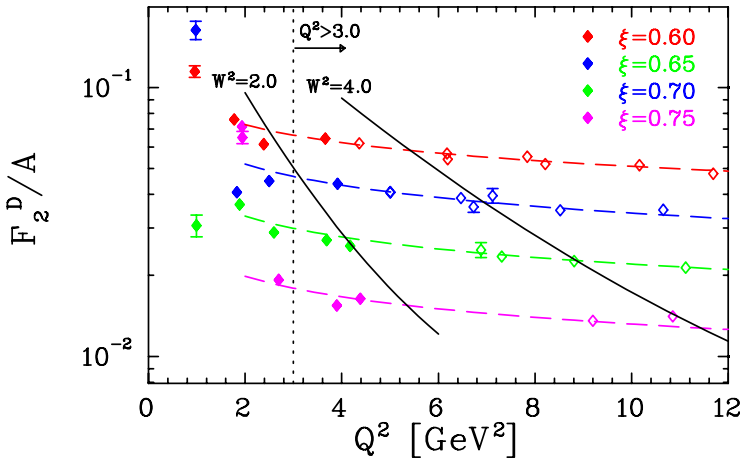

FIG. 8: Structure function for deuterium as a function of Q^2 at fixed ξ values. The solid lines indicate $W^2 > 2$ and $W^2 > 4$ GeV^2. Dashed lines show the logarithmic Q^2-dependence extracted from SLAC data at large Q^2.

The deviations from the pQCD evolution as determined by the E89-008 data are not precisely mapped out, but are largest for the lowest W^2 values where the quasielastic contributions dominate the higher twist contributions. At $Q^2 \approx 3$ GeV^2, the deviations from pQCD were found to be ≈10%. For E89-008, the EMC ratios were extracted above $Q^2 = 3$ GeV^2 so higher twist effects should be somewhat smaller. In addition, any A-independent higher twist effects will cancel in the EMC ratio. Because of the higher Q^2 and partial cancellation between targets, we believe that the uncertainties in the EMC ratio will be reduced by at least a factor of two. Therefore, we expect the higher twist contributions in the EMC ratio from E89-008 to be less than 5%. In the region where precise data exist from SLAC, the data sets agree within their uncertainties, indicating that the deviations are 3% or less.

For the proposed measurement at 6 GeV beam energy, the data at a fixed ξ value will be taken at larger Q^2 values (4–7 GeV^2), and larger W^2, both of which should reduce the effect of higher twist contributions as compared to the E89-008 data. We can reach $\xi = 0.78$ if we stay above $W^2 = 2.0$ GeV^2, where we expect that the higher twist contributions will be extremely small. We can extend this to $\xi = 0.86$ by using data at lower W^2 values: down to 1.3 GeV^2, the lowest W^2 value for which the ratio was extracted by E89-008. While the higher twist contributions may be larger there, they should still be less than they were for the 4 GeV E89-008 data, where we estimated an effect of less than 5%. Even a 5% effect on the EMC ratio would be negligible compared to the $\gtrsim 20\%$ statistical uncertainties on the existing data at large x. So for the kinematics proposed here, the extension of the measurements to $W^2 < 4$ should have a very small contribution to the uncertainties in the region where high-precision data already exists, and still be much smaller than the statistical uncertainties of the existing data at larger ξ values.

Finally, we will take a small amount of data so that we can map out the higher twist effects in the nuclear structure functions. This will lend further confidence that our data can be interpreted in a DIS–like framework. At large ξ values, we will make a quantitative determination of the higher twist contributions on the individual structure functions, and their A-dependence, which will allow us to make more precise estimates of their effects on

θ (deg)	E' (GeV)	x	Q^2 (GeV^2)	W^2 (GeV^2)	time (hours)
45	1.3-2.1 (3 settings)	0.5-1.0	4.4-7.3	0.9-5.3	112
20	3.4-4.3 (2 settings)	0.5-1.0	2.5-3.1	0.9-3.3	4
25	2.7-3.8 (2 settings)	0.5-1.0	3.1-4.2	0.9-3.9	4
30	2.2-3.2 (3 settings)	0.5-1.0	3.6-5.2	0.9-4.4	7
35	1.8-2.8 (3 settings)	0.5-1.0	3.9-6.0	0.9-4.8	9

TABLE I: Kinematics for the proposed measurements. All data will be taken at 6 GeV beam energy. The run time includes time for all nine targets at 45 degrees and three targets at 20, 25, 30, and 35 degrees. Additional time for dummy running and overhead for target and momentum changes is also included.

the EMC ratio. As noted above, at 4 GeV, we observe that the scaling violations in the structure functions are <10% for $Q^2 > 3$ GeV^2, and that since it is likely that the violations are similar regardless of target, they will be $< 5\%$ in the EMC ratio. However, these are conservative estimates, and we expect that the scaling violations will likely be smaller. For the 6 GeV measurements proposed here, we will take data at both higher Q^2 and higher W^2, further decreasing the higher twist contributions.

III. EXPERIMENTAL REQUIREMENTS

We propose a measurement of inclusive electron scattering from deuterium and several nuclei spanning ^{7}Li to ^{197}Au. Scattered electrons will be measured in the HMS and SOS spectrometers, which will run independently. The majority of the data will be taken in the HMS, while the SOS will be used to make measurements of electrons from background (charge symmetric) processes and to take additional data at the largest Q^2 values. All data will be taken at the highest beam energy available (6 GeV has been assumed for the proposed kinematics, however we do have a certain degree of flexibility regarding the exact beam energy). We will take data at 45 degrees, over a range of scattered electron energies covering $0.5 < x < 1.0$ in 20 bins. Data will be taken on deuterium, lithium, beryllium, carbon, aluminum, calcium, copper, silver, and gold, as well as a separate, dummy aluminum target (for subtraction of the target endcap contributions). Data will be taken at four additional angles for a subset of targets (deuterium, ^{12}C, and ^{63}Cu) to check the Q^2-dependence of the extracted EMC ratio. We will also take hydrogen elastic data for calibration at each angle setting. This measurement uses the standard Hall C spectrometers and detector packages. The hydrogen and deuterium cryotargets are standard Hall C equipment.

Table I lists the kinematics we propose to measure, corresponding to the kinematics shown

Activity	Time (hours)
Production Running	136
Target Boiling Studies	4
Angle Changes (4)	4
e^+ measurements	8
BCM calibrations	8
Beam spot monitoring	4
checkout/calibration	24
Total	188 (8 days)

TABLE II: Beam time request for the proposed experiment. The time shown is for HMS running. The SOS will be used for more extensive measurements of the pion and charge symmetric backgrounds at lower momenta, where they are most likely to be a non-negligible contribution. The SOS will also be used for parasitic data taking at larger angles (Q^2), if the backgrounds are tolerable at these kinematics.

in Fig. 6. Target and momentum changes are included in the total time at each scattering angle. In all cases, data will be obtained utilizing 4 cm deuterium, an aluminum 'dummy' target and several solid targets. Most of the solid targets that will be used have been used in previous Hall C experiments. One notable exception is the ^{7}Li target. For this target only, we will require that the target be in thermal contact with the cryotarget ladder, rather than be placed on a separate solid target ladder as is commonly done in Hall C. This will allow us to run higher currents without undo heating of the lithium target material. Even so, we estimate that we will be able to run at most 25 μA on a rather thin (100 mg/cm^2) target.

We will run at currents between 25 and 100 μA with 6 GeV beam energy. Table II is a summary of the beam time required for the measurement. Run times have been estimated assuming at least 1% statistics in each x bin for each target (double statistics for deuterium, which generally has a shorter run time). In addition to the data acquisition time, we have allocated time for checkout and background measurements, and spectrometer angle changes.

One of the possible backgrounds for the measurement is electrons coming from charge symmetric processes such as the decay of neutral pions or pair production. We will make measurements of positrons in order to subtract the charge symmetric background. JLab experiment E89-008 was run at 4 GeV over a similar range of angles. For a scattering angle of 55°, they saw a maximum e^+/e^- ratio of 15%. However, this was for $x > 1$ and a thick, high Z target. At lower x values, the e^+/e^- ratio was typically at or below 10% for the thick target. SLAC experiment E139 ran at higher energies (8-25 GeV) and found that the charge symmetric background was negligible for most of their kinematics, and largest ($\approx$10% on deuterium) at their lowest x and Q^2 values ($x < 0.1$). We do not expect significant backgrounds except possibly at the lowest electron momentum settings and largest angle. Even for these kinematics, the corrections are likely to be small except for the heaviest targets, where a subtraction of the charge-symmetric background will suffice. Data will be

Source	Absolute Uncertainty	Relative Uncertainty	$\delta\sigma/\sigma(\%)$	$\delta R/R(\%)$ point-to-point	$\delta R/R(\%)$ scale	$\delta R/R$ (%) Statistical
HMS Momentum	<0.1%	0.01%	0.2	-	-	
Beam Energy	<0.1%	<0.02%	0.2	-	-	
θ	0.5mr	0.2mr	0.1	-	-	
Beam angle	0.5mr	0.1mr	0.1	-	-	
t_D	0.5%		0.5	-	0.5	
t_A	0.5–2.0%		0.5–2.0	-	0.5–2.0	
Charge	0.4%	0.2%	0.5	0.2	0.2	
Target Boiling	<0.5%	0.2%	<0.5	0.1	0.2	
Endcap Subtraction	<1.0%	0.2%	<1.0	0.1	0.1	
Acceptance	1.0-2.0%	0.2%	1.0-2.0	0.2	0.2	
Radiative Corrections	2.0%	0.5%	2.0	0.2–0.4	0.4	
Detector Efficiency	0.5%	0.2%	0.5	0.2	-	
Deadtime Correction	<0.5%	0.2%	<0.5	0.1	0.2	
Positron Background	0.2%	0.2%	0.2	0.1–0.3	0.2	
Total			2.5-3.2	0.5–0.6	0.9–2.2	0.3-1.2
E139			2.4-3.7	0.3-1.3	1.0-2.5	0.5-11.0

TABLE III: Systematic uncertainties in the ratio $\sigma_A/\sigma_{^2H}$, compared to E139 uncertainties. For $x < 0.9$, the statistical uncertainties will be 0.3–1.2%. The point–to–point systematic error in the target ratios will be 0.5–0.6% and the overall systematic error will range from 0.9–2.2%, depending on the target.

taken in the SOS to determine the charge-symmetric backgrounds at these kinematics.

Pions are the other main source of background for the measurement. For the E89-008 experiment, the combination of the lead glass shower counter and the gas Čerenkov detector in the HMS (and SOS) provides pion rejection at ≈15,000:1 for a pion momentum of 1.0 GeV/c, and almost 100,000:1 for momenta above 1.5 GeV/c. For the high momentum settings, this should be more than adequate to remove any pion contamination from the measurement. We will also have direct measurements of the pion backgrounds and can make corrections for pion contamination if there are kinematics where there is some small contamination left after the PID cuts.

We estimate a systematic uncertainty of 2.5-3.2% in the measured cross sections for most of the kinematics. To correct for density changes due to localized heating in the deuterium target, we will measure rate as a function of current. Many sources of uncertainty will cancel in the cross section ratios for different targets, and we estimate a final point–to–point systematic uncertainty in the ratios of approximately 0.6% and an overall scale systematic uncertainty of $0.9 - 2.2\%$. Table III shows the contributions to the systematic uncertainties in the target ratios. The solid targets will be measured at the same time as the deuterium target, and so will not have uncertainties in the EMC ratios due to uncertainties in the kinematics. However, they will have some uncertainty in the acceptance, due to the difference in the target length. Note that the uncertainty in the thickness of the deuterium target is a common uncertainty for the $\sigma_A/\sigma_{^2H}$ ratios for all targets.

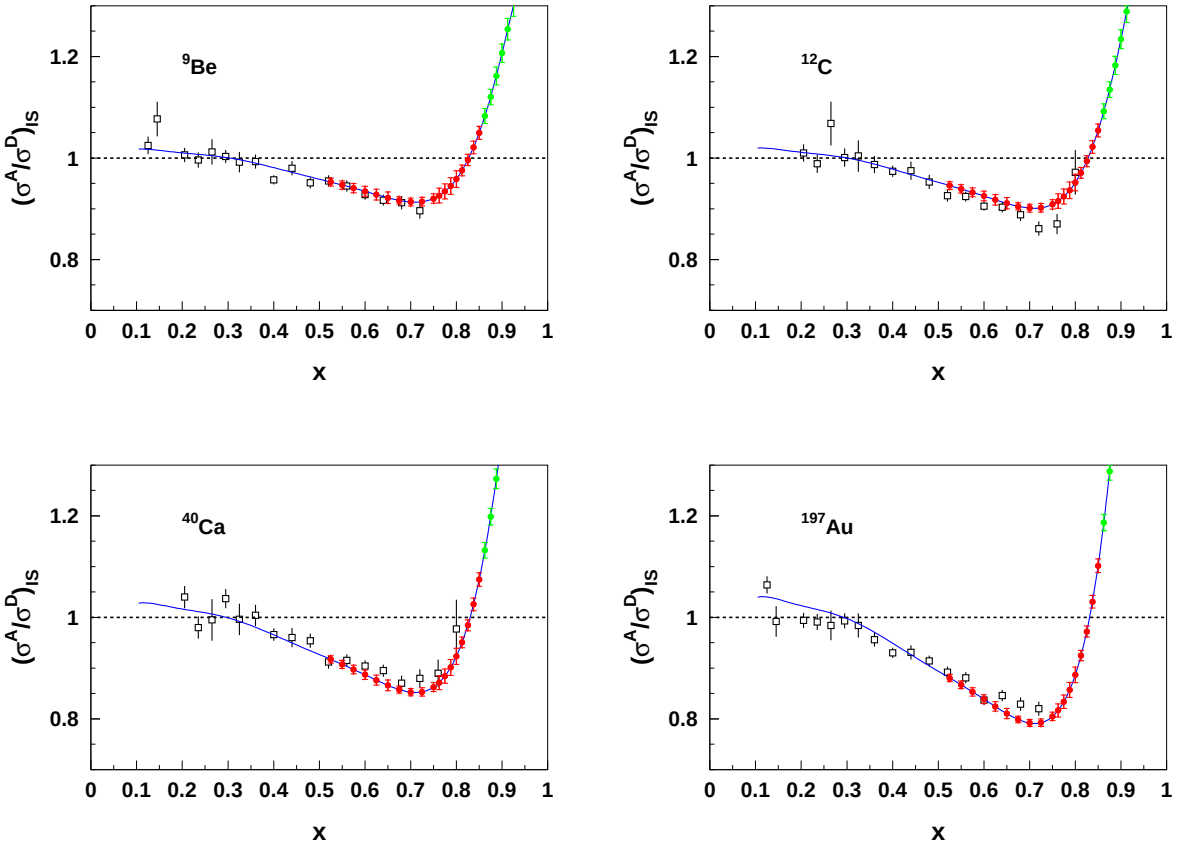

FIG. 9: Projected uncertainties for the ^{9}Be, ^{40}Ca, and ^{197}Au EMC ratios (solid circles). The inner error bars are statistical, while the outer errors are combined statistics and point–to–point errors. Not shown is an overall $\approx 1-2\%$ systematic uncertainty. The dark red (light green) points denote kinematics for which $W^2 > 2$ GeV^2 ($W^2 < 2$ GeV^2). The projected data have been shown in x–bins 0.0125 wide for $x > 0.75$ (rather than the default 0.025) to elucidate our sensitivity to the high x cross–over. Also shown are the data from SLAC E139 (open squares), along with their parameterization of the x-dependence (solid line). Note that some of our projected data points are off the scale at high x. The full data set will also include the EMC ratios from ^{7}Li, ^{12}C, ^{27}Al, ^{63}Cu, and ^{108}Ag with similar errors.

IV. SUMMARY

We request 8 days in Hall C to measure inclusive scattering from deuterium, ^{7}Li, ^{9}Be, ^{12}C, ^{27}Al, ^{40}Ca, ^{63}Cu, ^{108}Ag, ^{197}Au for x>0.5 and Q^2> 4.0 GeV^2. We will take additional data on a subset of these targets (deuterium, ^{12}C, and ^{63}Cu) to examine the Q^2-dependence of the nuclear structure functions and the EMC ratio. This measurement takes advantage of the observed equivalence of the EMC effect as measured in the canonical DIS regime and as measured in the resonance region. We will measure the EMC effect with high precision at high x, placing rigorous constraints on calculations of the EMC effect which must include binding and nuclear wave–function effects before being able to make any statements about

more exotic physics, such as multiquark clusters or rescaling of nucleon structure functions in nuclei. The high x region is particularly interesting in light of recent results that indicate that the high x cross–over increases as A increases, which contradicts the simple picture in which the rise of the EMC ratio at high x is simply due to Fermi motion and binding.

V. RELATION TO OTHER EXPERIMENTS

This proposal is complementary to approved experiment E03–103, "A Precise Measurement of the Nuclear Dependence of Structure Functions in Light Nuclei" [25]. The focus of that proposal is on measuring the EMC effect in ^{3}He and ^{4}He over a broad range of x. The main goal of E03–103 is to extend measurements of the EMC effect (and nuclear structure functions) to few-body nuclei, where more advanced, few-body calculations can be performed. The goal of this proposal is to extend measurements of the EMC effect to larger x values than existing data, to study the A-dependence of the shape of the EMC effect, and to provide better data for evaluating and constraining models of the binding and Fermi motion components of the EMC effect, which are important over a wide range of x. Thus, this proposal is focused on high-x, and on covering a range of nuclei. This proposal does not include ^{3}He and ^{4}He, as high-x data for these nuclei will be obtained as part of the E03–103 measurement.

This proposal is also similar to PR94-105, which was proposed to PAC 9. That proposal included both ^{3}He, ^{4}He, and a range of heavier nuclei. The goal was to improve on the existing measurements of the EMC effect by making precise measurements on ^{3}He and ^{4}He, and by measuring both F_2 and $R = \sigma_L/\sigma_T$. However, there is very little overlap with the kinematics of this proposal, because PR94-105 was focused on measurements in the DIS region, and so covered $0.1 < x < 0.6$, while this proposal focuses on the high-x region, $x > 0.5$.

Acknowledgments

This work was supported by the U. S. Department of Energy, Nuclear Physics Division, under contracts W-31-109-ENG-38 and DE-AC05-84ER40150.

---

[1] J. Aubert et al., Phys. Lett. B **123**, 275 (1983).
[2] D. F. Geesaman, K. Saito, and A. W. Thomas, Ann. Rev. Nucl. Sci. **45**, 337 (1995).
[3] P. R. Norton, Rept. Prog. Phys. **66**, 1253 (2003).
[4] A. C. Benvenuti et al. (BCDMS), Phys. Lett. **B189**, 483 (1987).
[5] A. Bodek et al., Phys. Rev. Lett. **50**, 1431 (1983).
[6] J. Gomez et al., Phys. Rev. D **49**, 4348 (1994).
[7] D. S. Koltun, Phys. Rev. Lett. **28**, 182 (1972).
[8] A. Bodek and J. L. Ritchie, Phys. Rev. **D23**, 1070 (1981).
[9] A. Bodek and J. L. Ritchie, Phys. Rev. **D24**, 1400 (1981).
[10] E. Marco, E. Oset, and P. Fernandez de Cordoba, Nucl. Phys. **A611**, 484 (1996).
[11] F. Gross and S. Liuti, Phys. Rev. **C45**, 1374 (1992).

[12] C. W. De Jager, H. De Vries, and C. De Vries, Atom. Data Nucl. Data Tabl. **14**, 479 (1974).
[13] J. Arrington, R. Ent, C. E. Keppel, J. Mammei, and I. Niculescu (2003), nucl-ex/0307012.
[14] H. Georgi and H. D. Politzer, Phys. Rev. D **14**, 1829 (1976).
[15] I. Niculescu et al., Phys. Rev. Lett. **85**, 1186 (2000).
[16] I. Niculescu, Ph.D. thesis, Hampton University (1999).
[17] J. Arrington et al., Phys. Rev. **C64**, 014602 (2001).
[18] A. D. Martin, R. G. Roberts, W. J. Stirling, and R. S. Thorne, Eur. Phys. J. **C28**, 455 (2003).
[19] M. Arneodo et al. (New Muon.), Phys. Lett. **B364**, 107 (1995).
[20] L.W.Whitlow et al., Phys. Lett. B **282**, 475 (1992).
[21] C. Keppel, private communication.
[22] C. S. Armstrong et al., Phys. Rev. **D63**, 094008 (2001).
[23] G. Ricco et al., Phys. Rev. C **57**, 356 (1998).
[24] B. W. Filippone et al., Phys. Rev. C **45**, 1582 (1992).
[25] J. Arrington et al., Jefferson lab experiment E03-103.